Inorganic Chemistry
Article

Inorg. Chem. **2010**, *49*, 4447–4457 **4447**
DOI: 10.1021/ic902300c

Thiomethoxychalcone-Functionalized Ferrocene Ligands as Selective Chemodosimeters for Mercury(II): Single-Crystal X-ray Structural Signature of the $[Hg_8(\mu_8\text{-}S)(SCH_3)_{12}]^{2+}$ Cluster

B. Nisar Ahamed, M. Arunachalam, and Pradyut Ghosh*

Department of Inorganic Chemistry, Indian Association for the Cultivation of Science, 2A & 2B Raja S. C. Mullick Road, Kolkata 700032, India.

Received November 20, 2009

Thiomethoxychalcone-based ligands bis[3,3-bis(methylsulfanyl)]-1,1′- η^5-ferrocenyl-2-propen-1-one ($\mathbf{L^1}$), 3,3-bis-(methylsulfanyl)-1-η^5-ferrocenyl-2-propen-1-one ($\mathbf{L^2}$), and 3-methylsulfanyl-3-sulfanyl-1-η^5-ferrocenyl-2-propen-1-one ($\mathbf{L^3}$) have been synthesized on the ferrocene backbone by varying the number of chalcone arms and thiomethoxy substitutents. The single-crystal X-ray crystallographic analyses of all three ligands are reported in which crystals of $\mathbf{L^1}$ were obtained as both syn and anti conformers and showed the conformational freedom of the two cyclopentadienyl (Cp) units. $\mathbf{L^1}$−$\mathbf{L^3}$ are studied extensively toward their applicability in the colorimetric sensing of metal ions in solution. The solution-state study of mono- and bis(thiomethoxy)ferrocenylchalcone-functionalized ligands $\mathbf{L^1}$ and $\mathbf{L^2}$ showed selective colorimetric sensing for Hg^{2+} over Li^+, Na^+, Ca^{2+}, Mg^{2+}, Cr^{2+}, Mn^{2+}, Fe^{2+}, Co^{2+}, Ni^{2+}, Cu^{2+}, Zn^{2+}, Cd^{2+}, and Au^{3+} in acetonitrile. In both cases, a selective color change from orange to purple was observed with Hg^{2+} and the resultant solution showed the appearance of a new peak at 565 nm (ε=3920 M^{-1} cm^{-1}) for $\mathbf{L^1}$ and 600 nm (ε=1140 M^{-1} cm^{-1}) for $\mathbf{L^2}$ in the UV/vis experiments. The UV/vis titration profiles of $\mathbf{L^1}$ and $\mathbf{L^2}$ indicate the formation of 2:1 ($\mathbf{L^1}$/Hg^{2+}) and 1:1 ($\mathbf{L^2}$/Hg^{2+}) initial complexations in solution. On the other hand, $\mathbf{L^3}$ with thiomethoxy- and thiol-functionalized ferrocenylchalcone showed no appreciable color change with Hg^{2+} under the same experimental conditions. Attempts were made to isolate single crystals of the resulting purple solution obtained in the cases of $\mathbf{L^1}$ and $\mathbf{L^2}$ with Hg^{2+}. In both cases, crystals suitable for a single-crystal X-ray diffraction study were isolated in very low yield by a layer diffusion technique. The single-crystal structural investigations demonstrated the formation of a sulfide-encapsulated mercury thiolate cubo-ctahedron cluster, $[Hg_8S(SCH_3)_{12}]^{2+}$, upon a selective chemodosimetric desulfurization reaction between Hg^{2+} and $\mathbf{L^1}$ or $\mathbf{L^2}$. Cyclic voltammetric studies also support the Hg^{2+}-induced cleavage of thiomethoxy groups.

Introduction

Chemical sensing of mercury is of great importance because of its tremendously toxic impact on the environment as well as in biological systems.[1] The extreme toxicity of mercury and its derivatives toward biological systems results from its high affinity for thiol groups in proteins and enzymes, leading to the dysfunction of cells and, consequently, causing serious damage to the central nervous and endocrine systems.[1a−c] Efforts have been made to develop various chemosensors for the detection of Hg^{2+}.[2] Recently, there is immense interest in chemodosimeter-based chemical sensing through a specific irreversible chemical reaction between dosimetric molecules and target species, leading to a fluorescent/color change in the receptor.[2d,3] Different systems that have been developed as chemodosimeters for Hg^{2+} are based on different reaction mechanisms like hydrolysis,[3a−c] cyclization,[3d−h] ring opening,[3i−r] mercuration,[3s] desulfurization[3t−v] and elimination.[3w,x] Most chemodosimeters developed so far have been designed by choosing the fluorogenic or chromogenic unit as a backbone and, related to their emission or color changes, monitored upon metal ion introduction.[2d,3] Moreover, reports on the single-crystal X-ray crystallographic characterization of chemodosimetric sensing via different mechanisms are very rare.[4] The structural

*To whom correspondence should be addressed. E-mail: icpg@iacs.res.in.

(1) (a) Sunshine, H. R.; Lippard, S. J. *Nucleic Acids Res.* **1974**, *1*, 673–688. (b) Sekowski, J. W.; Malkas, L. H.; Wei, Y. T.; Hickey, R. J. *Toxicol. Appl. Pharmacol.* **1997**, *145*, 268–276. (c) Onyido, I.; Norris, A. R.; Buncel, E. *Chem. Rev.* **2004**, *104*, 5911–5929. (d) Fitzgerald, W. F.; Lamborg, C. H.; Hammerschmidt, C. R. *Chem. Rev.* **2007**, *107*, 641–662.

(2) (a) Nolan, E. M.; Lippard, S. J. *Chem. Rev.* **2008**, *108*, 3443–3480. (b) Kim, H. N.; Lee, M. H.; Kim, H. J.; Kim, J. S.; Yoon, J. *Chem. Soc. Rev.* **2008**, *37*, 1465–1472. (c) Beija, M.; Afonso, C. A. M.; Martinho, J. M. G. *Chem. Soc. Rev.* **2009**, *38*, 2410–2433. (d) Suresh, M.; Mishra, S. K.; Mishra, S.; Das, A. *Chem. Commun.* **2009**, 2496–2498. (e) Yoon, S.; Miller, E. W.; He, Q.; Do, P. H.; Chang, C. J. *Angew. Chem., Int. Ed.* **2007**, *46*, 6658–6661. (f) Li, H.-W.; Li, Y.; Dang, Y.-Q.; Ma, L.-J.; Wu, Y.; Hou, G.; Wu, L. *Chem. Commun.* **2009**, 4453–4455. (g) Che, Y.; Yang, X.; Zang, L. *Chem. Commun.* **2008**, 1413–1415. (h) Wang, J.; Liu, B. *Chem. Commun.* **2008**, 4759–4761. (i) Yuan, M.; Li, Y.; Li, J.; Li, C.; Liu, X.; Lv, J.; Xu, J.; Liu, H.; Wang, S.; Zhu, D. *Org. Lett.* **2007**, *9*, 2313–2316. (j) Zhu, Z.; Su, Y.; Li, J.; Li, D.; Zhang, J.; Song, S.; Zhao, Y.; Li, G.; Fan, C. *Anal. Chem.* **2009**, *81*, 7660–7666. (k) Pandey, S.; Azam, A.; Pandey, S.; Chawla, H. M. *Org. Biomol. Chem.* **2009**, *7*, 269–279. (l) Dhir, A.; Bhalla, V.; Kumar, M. *Org. Lett.* **2008**, *10*, 4891–4894. (m) Ahamed, B. N.; Ravikumar, I.; Ghosh, P. *New J. Chem.* **2009**, *33*, 1825–1828.

Published on Web 04/22/2010

chemistry of biological metal−sulfur clusters is remarkable because of their complexity and variety.[5a−c] Metallothioneins are cysteine-rich metalloregulatory proteins that bind a wide range of metals both in vivo and in vitro.[5d−h] Despite similarities between the chemistry of cadmium, zinc, copper, and mercury, the structural model for a mercury-containing metallothionein is not well established.[5a] Mercury thiolate clusters are of great importance because these clusters emerge greatly by the importance of these complexes as structural models in the detoxification of mercury by metallothioneins in proteins.[5a] Therefore, efforts have been made to develop various metal thiolate compounds to understand the binding of proteins toward toxic metal ions.[5i−k] Further, there is immense interest in complete cubane or incomplete cubane frameworks because of the interest in their geometrical relevance to the active site structures of enzymes with a cubanelike unit.[6] Few examples of cubic clusters are known that contain edge-bridged ligands with a direct M−M bond and an anion-encapsulated edge-bridged cube.[7] The ferrocene backbone is a useful potentially applicable moiety for incorporating redox functions into supramolecular complexes that can exhibit interaction with electrophilic Hg^{2+} either by iron or by a ring.[8] Herein, we introduce thiomethoxychalcones functionalized on ferrocene, **L**^{1} and **L**^{2}, as selective colorimeric chemosensors for Hg^{2+} in solution. We also demonstrate the single-crystal X-ray structure of a sulfide-encapsulated distorted cuboctahedron mercury thiolate cluster, $[Hg_8(\mu_8\text{-}S)(SCH_3)_{12}]^{2+}$ (**1**), as one of the chemodosimetric products. To the best of our knowledge and according to a review by Henkel and Krebs, no such example of an octanuclear $[M_8S(SR)_{12}]^{2+}$ metal−sulfur framework for a divalent metal ion in coordination chemistry is known.[5a,9]

Experimental Section

Materials and Methods. Perchlorate salts of Li^+, Na^+, Ca^{2+}, Mg^{2+}, Cr^{2+}, Mn^{2+}, Fe^{2+}, Co^{2+}, Cu^{2+}, Zn^{2+}, Cd^{2+}, and Hg^{2+} and a nitrate salt of Ni^{2+} purchased from Aldrich and $HAuCl_4$ purchased from SRL (New Delhi, India) were used directly without further purification. Ferrocene, acetyl chloride, aluminum chloride, potassium *tert*-butoxide (*t*-BuOK), carbon disulfide (CS_2), methyl iodide (CH_3I), chloroform ($CHCl_3$), dichloromethane (CH_2Cl_2), acetonitrile (CH_3CN), petroleum ether, diethyl ether, and tetrahydrofuran (THF) were purchased from Cyno Chem Inc. (Ahmedabad, India). Solvents were dried by conventional methods and distilled under a N_2 atmosphere before use. 1-Monoacetylferrocene[10a] and 1,1′-diacetylferrocene[10b] were synthesized as per literature procedures. **L**^{2} was synthesized by a slightly modified literature procedure.[10c]

Instrumentation. ^{1}H and ^{13}C NMR spectra were recorded on Bruker 300 and 75 MHz FT-NMR spectrometers, respectively, using tetramethylsilane as the internal reference. Electrospray ionization mass spectrometry (ESI-MS) measurements were carried out on a Qtof Micro YA263 HRMS instrument. The absorption spectra were recorded with a Perkin-Elmer Lambda 950 UV/vis/near-IR (NIR) scanning spectrophotometer at 298 K. The cyclic voltammetric (CV) measurements were performed on a Princeton Applied Research potentiostat/galvonostat model 273A. Elemental analyses for the synthesized ligands and complexes were carried out with a 2500 series II elemental analyzer (PerkinElmer, Waltham, MA). Thermogravimetric analysis (TGA) was performed using an SDT Q600 V8.2 Build 100 thermal analyzer. ***Caution!*** *Metal perchlorate salts are potentially explosive in certain conditions. All due precautions should be taken while handling perchlorate salts.*

Designing Aspects of Ferrocenylchalcones L^{1}−L^{3}. For a receptor to bind with the specific guest, it should possess complementary binding sites. The designing principles of **L**^{1}−**L**^{3} are as follows: (1) The ferrocene backbone is a potentially useful

(3) (a) Song, K. C.; Kim, J. S.; Park, S. M.; Chung, K.-C.; Ahn, S.; Chang, S.-K. *Org. Lett.* **2006**, *8*, 3413–3416. (b) Chae, M. Y.; Czarnik, A. W. *J. Am. Chem. Soc.* **1992**, *114*, 9704–9705. (c) Zhang, G.; Zhang, D.; Yin, S.; Yang, X.; Shuaia, Z.; Zhu, D. *Chem. Commun.* **2005**, 2161–2163. (d) Kim, H. J.; Lee, S. J.; Park, S. Y.; Jung, J. H.; Kim, J. S. *Adv. Mater.* **2008**, *20*, 3229–3234. (e) Lee, M. H.; Cho, B.-K.; Yoon, J.; Kim, J. S. *Org. Lett.* **2007**, *9*, 4515–4518. (f) Wu, F.-Y.; Zhao, Y.-Q.; Ji, Z.-J.; Wu, Y.-M. *J. Fluoresc.* **2007**, *17*, 460–465. (g) Wu, J.-S.; Hwang, I.-C.; Kim, K. S.; Kim, J. S. *Org. Lett.* **2007**, *9*, 907–910. (h) Liu, B.; Tian, H. *Chem. Commun.* **2005**, 3156–3158. (i) Yang, Y.-K.; Yook, K.-J.; Tae, J. *J. Am. Chem. Soc.* **2005**, *127*, 16760–16761. (j) Suresh, M.; Mishra, S.; Mishra, S. K.; Suresh, E.; Mandal, A. K.; Shrivastav, A.; Das, A. *Org. Lett.* **2009**, *11*, 2740–2743. (k) Zhang, X.; Xiao, Y.; Qian, X. *Angew. Chem., Int. Ed.* **2008**, *47*, 8025–8029. (l) Jana, A.; Kim, J. S.; Jung, H. S.; Bharadwaj, P. K. *Chem. Commun.* **2009**, 4417–4419. (m) Suresh, M.; Shrivastav, A.; Mishra, S.; Suresh, E.; Das, A. *Org. Lett.* **2008**, *10*, 3013–3016. (n) Du, J.; Fan, J.; Peng, X.; Sun, P.; Wang, J.; Li, H.; Sun, S. *Org. Lett.* **2010**, *12*, 476–479. (o) Huang, J.; Xu, Y.; Qian, X. *J. Org. Chem.* **2009**, *74*, 2167–2170. (p) Shi, W.; Sun, S.; Li, X.; Ma, H. *Inorg. Chem.* **2010**, *49*, 1206–1210. (q) Zhan, X.-Q.; Qian, Z.-H.; Zheng, H.; Su, B.-Y.; Lan, Z.; Xu, J.-G. *Chem. Commun.* **2008**, 1859–1861. (r) Shi, W.; Ma, H. *Chem. Commun.* **2008**, 1856–1858. (s) Choi, M. G.; Ryu, D. H.; Jeon, H. L.; Cha, S.; Cho, J.; Joo, H. H.; Hong, K. S.; Lee, C.; Ahn, S.; Chang., S.-K. *Org. Lett.* **2008**, *10*, 3717–3720. (t) Choi, M. G.; Kim, Y. H.; Namgoong, J. E.; Chang, S.-K. *Chem. Commun.* **2009**, 3560–3562. (u) Ros-Lis, J. V.; Marcos, M. D.; Matinez-Máñez, R.; Rurack, K.; Soto, J. *Angew. Chem., Int. Ed.* **2005**, *44*, 4405–4407. (v) Jiang, W.; Wang, W. *Chem. Commun.* **2009**, 3913–3915. (w) Song, F.; Watanabe, S.; Floreancig, P. E.; Koide, K. *J. Am. Chem. Soc.* **2008**, *130*, 16460–16461. (x) Santra, M.; Ryu, D.; Chatterjee, A.; Ko, S.-K.; Shin, I.; Ahn, K. H. *Chem. Commun.* **2009**, 2115–2117.

(4) (a) Chen, X.; Nam, S.-W.; Jou, M. J.; Kim, Y.; Kim, S.-J.; Park, S.; Yoon, J. *Org. Lett.* **2008**, *10*, 5235–5238. (b) Zhao, Y.; Lin, Z.; He, C.; Wu, H.; Duan, C. *Inorg. Chem.* **2006**, *45*, 10013–10015. (c) Lee, M. H.; Lee, S. W.; Kim, S. H.; Kang, C.; Kim, J. S. *Org. Lett.* **2009**, *11*, 2101–2104. (d) Huang, W.; Zhu, X.; Wua, D.; He, C.; Hu, X.; Duan, C. *Dalton Trans.* **2009**, 10457–10465.

(5) (a) Henkel, G.; Krebs, B. *Chem. Rev.* **2004**, *104*, 801–824. (b) Dance, I. G. *J. Am. Chem. Soc.* **1980**, *102*, 3445–3451. (c) Dance, I. G. *Inorg. Chem.* **1981**, *20*, 1487–1492. (d) Stillman, M. J. *Coord. Chem. Rev.* **1995**, *144*, 461–511. (e) Holm, R. H.; Kennepohl, P.; Solomon, E. I. *Chem. Rev.* **1996**, *96*, 2239–2314. (f) Gonzàlez-Duarte, P.; Clegg, W.; Casals, I.; Sola, J.; Rius, J. *J. Am. Chem. Soc.* **1998**, *120*, 1260–1266. (g) Coyle, P.; Philcoxa, J. C.; Careya, L. C.; Rofea, A. M. *Cell. Mol. Life Sci.* **2002**, *59*, 627–647. (h) Lu, W.; Zelazowski, A. J.; Stillman, M. J. *Inorg. Chem.* **1993**, *32*, 919–926. (i) Melnick, J. G.; Parkin, G. *Science* **2007**, *317*, 225–227. (j) Melnick, J. G.; Yurkerwich, K.; Parkin, G. *Inorg. Chem.* **2009**, *48*, 6763–6772. (k) Krebs, B.; Henkel, G. *Angew. Chem., Int. Ed. Engl.* **1991**, *30*, 769–788.

(6) (a) Zhang, Y.; Holm, R. H. *J. Am. Chem. Soc.* **2003**, *125*, 3910–3920. (b) Rao, P. V.; Holm, R. H. *Chem. Rev.* **2004**, *104*, 527–559. (c) Kure, B.; Ogo, S.; Inoki, D.; Nakai, H.; Isobe, K.; Fukuzumi, S. *J. Am. Chem. Soc.* **2005**, *127*, 14366–14374.

(7) (a) Stephan, H.-O.; Chen, C.; Henkel, G.; Griesarb, K.; Haase, W. *J. Chem. Soc., Chem. Commun.* **1993**, 886–888. (b) Fackler, J. P., Jr. *Inorg. Chem.* **2002**, *41*, 6959–6972. (c) Zheng, N.; Bu, X.; Feng, P. *J. Am. Chem. Soc.* **2002**, *124*, 9688–9689. (d) Lobana, T. S.; Wang, J.-C.; Liu, C. W. *Coord. Chem. Rev.* **2007**, *251*, 91–110. (e) Zhang, Z.; Zhang, J.; Wu, T.; Bu, X.; Feng, P. *J. Am. Chem. Soc.* **2008**, *130*, 15238–15239. (f) Zhang, Q.; Lin, Z.; Bu, X.; Wu, T.; Feng, P. *Chem. Mater.* **2008**, *20*, 3239–3241. (g) Liao, P.-K.; Sarkar, B.; Chang, H.-W.; Wang, J.-C.; Liu, C. W. *Inorg. Chem.* **2009**, *48*, 4089–4097.

(8) (a) Silver, J. *J. Chem. Soc., Dalton Trans.* **1990**, 3513–3516. (b) Cunningham., A. F., Jr. *Organometallics* **1997**, *16*, 1114–1122. (c) Sünkel, K.; Kiessling, T. *J. Organomet. Chem.* **2001**, *637−639*, 796–799.

(9) A Cambridge Structural Database (CSD) search (CSD version 5.31, Nov 2009 updates) was performed with a 12 thiolate-bridged octanuclear metal thiolate clusters $[M_8S_{12}]$ having the geometry as found in the single-crystal structure of **1** without any restriction. The search revealed 106 hits, and most of them are anionic clusters or different cluster compositions where $[M_8S_{12}]$ is embedded. Careful analysis showed only one cationic $[M_8(SR)_{12}]^{4+}$ cluster that encapsulated SO_4^{2-} inside the cage with the composition of $[M_8(SO_4)(SR)_{12}]^{2+}$ (refcode EGIFUV[7c]) .

(10) (a) Lam, W.-S.; Kok, S. H. L.; Au-Yeung, T. T.-L.; Wu, J.; Cheung, H.-Y.; Lam, F.-L.; Yeung, C.-H.; Chan, A. S. C. *Adv. Synth. Catal.* **2006**, *348*, 370–374. (b) Carroll, M. A.; White, A. J. P.; Widdowson, D. A.; William, D. J. *J. Chem. Soc., Perkin Trans. 1* **2000**, 1551–1557. (c) Rao, H. S. P.; Sivakumar, S. *J. Org. Chem.* **2006**, *71*, 8715–8723.

moiety to incorporate redox functionality, which upon binding with analyte(s) can exhibit changes in the redox potential of the ferrocene−ferrocenium couple by electrostatic communication.[11] (2) Functionalized ketene *S*,*S*-acetals are versatile intermediates in organic synthesis, and electron-withdrawing group-appended ketene *S*,*S*-acetals are of particular importance because of their highly polarized push−pull interaction.[10c,12] (3) Hg^{2+} shows a high affinity toward sulfur atoms because of its highly thiophilic nature; therefore, a ketene *S*,*S*-acetal functionality could be useful for detection of this ion. In these chalcones, the thiomethoxy group is covalently bound to a redox-active chromogenic ferrocene moiety via an α,β-unsaturated carbonyl linker. While binding with Hg^{2+}, a highly polarized push−pull interaction on the C=C bond can exhibit a change in the spectroscopic and redox potentials of the ferrocene−ferrocenium couple by electrostatic communication. Considering the above points, we have designed and synthesized ligands $\mathbf{L^1}$−$\mathbf{L^3}$ having various numbers of thiomethoxy functionalities on ferrocenylchalcone.

Syntheses of Ferrocenylchalcones $\mathbf{L^1}$−$\mathbf{L^3}$. In the case of $\mathbf{L^1}$, a mixture of 1,1′-diacetylferrocene (9.0 mmol) and CS_2 (22 mmol) in dry THF (30 mL) was added through a pressure equalizer funnel into the suspension of *t*-BuOK (62 mmol) in dry THF (20 mL) at 0 °C with vigorous stirring for ∼90 min. The appearance of a reddish solid in the reaction mixture indicated the formation of tetrapotassium salt of 1,1′-ferrocenyl-3,3-disulfanyl-2-propen-1-one. To this suspension was carefully added dropwise for 15 min at 0 °C a solution of CH_3I (21.6 mmol) in dry THF (15 mL), and the reaction mixture was allowed to stir at 0 °C for another 90 min. After completion of the reaction (thin-layer chromatography; chloroform), the mixture was transferred into a 500 mL beaker containing 250 g of crushed ice, and the contents of the beaker was stirred. The reddish-yellow solid formed was filtered and washed with water (3 × 100 mL). The crude solid was recrystallized from CH_2Cl_2/diethyl ether (1:1), resulting in *syn*-$\mathbf{L^1}$, whereas recrystallization from CH_2Cl_2/petroleum ether (1:1) resulted in *anti*-$\mathbf{L^1}$. Two other chalcone ligands, $\mathbf{L^2}$ and $\mathbf{L^3}$, were prepared following the procedure adopted in the case of $\mathbf{L^1}$, where *t*-BuOK (31.05 mmol), monoacetylferrocene (9.0 mmol), and CS_2 (10.8 mmol) were used in both cases, whereas 10.8 and 5.4 mmol of CH_3I were used for $\mathbf{L^2}$ and $\mathbf{L^3}$, respectively. In both cases, the crude solid was recrystallized from CH_2Cl_2, in which pink plate crystals of $\mathbf{L^2}$ and pink block crystals of $\mathbf{L^3}$ were isolated.

$\mathbf{L^1}$. Yield: 52%. ^{1}H NMR (300 MHz, $CDCl_3$): δ 6.17 (s, 2H), 4.72 (t, 4H), 4.43 (t, 4H), 2.54 (s, 6H), 2.48 (s, 6H). ^{13}C NMR (75 MHz, DMSO-d_6): δ 187.47, 161.91, 111.42, 83.52, 73.23, 70.89, 17.16, 14.78. ESI-MS data: 478.8769 ($[M]^+$), 500.8546 ($[M + Na]^+$). Anal. Calcd for $C_{20}H_{22}FeO_2S_4$: C, 50.20; H, 4.63; S, 26.81. Found: C, 50.02; H, 4.45, S, 26.58.

$\mathbf{L^2}$. Yield: 61%. ^{1}H NMR (300 MHz, $CDCl_3$): δ 6.34 (s, 1H), 4.78 (s, 2H), 4.45 (s, 2H), 4.17 (s, 5H), 2.53 (s, 3H), 2.50 (s, 3H). ^{13}C NMR (75 MHz, $CDCl_3$): δ 189.51, 161.14, 111.47, 81.75, 71.81, 69.97, 69.24, 17.44, 15.12. ESI-MS data: 332.6512 ($[M]^+$), 354.6112 ($[M + Na]^+$). Anal. Calcd for $C_{15}H_{16}FeOS_2$: C, 54.22; H, 4.85; S, 19.3. Found: C, 54.02; H, 4.73; S, 19.16.

$\mathbf{L^3}$. Yield: 43%. ^{1}H NMR (300 MHz, $CDCl_3$): δ 15.07 (s, 1H), 6.61 (s, 1H), 4.82 (s, 2H), 4.55 (s, 2H), 4.22 (s, 5H), 2.62 (s, 3H). ^{13}C NMR (75 MHz, DMSO-d_6): δ 212.49, 176.48, 107.59, 72.23, 70.61, 68.25, 16.79. ESI-MS data: 319.0377 ($[M]^+$), 340.9876 ($[M + Na]^+$). Anal. Calcd for $C_{14}H_{14}FeOS_2$: C, 52.84; H, 4.43; S, 20.15. Found: C, 52.77; H, 4.23; S, 19.8.

Mercury Thiolate Cluster 1. The ligand $\mathbf{L^1}$ (25 mg) or $\mathbf{L^2}$ (25 mg) was dissolved in 25 mL of CH_2Cl_2 and was layered with 25 mL of a CH_3CN solution containing 20 mg of $Hg(ClO_4)_2$, and the mixture was allowed to diffuse slowly at room temperature. Upon slow diffusion of $Hg(ClO_4)_2$ into the ligand solution, stepwise color changes were observed from purple to blackish brown via brown. After a week, a few purple prismlike crystals suitable for single-crystal X-ray crystallographic analysis were obtained in the resulting blackish residue. Single crystals of **1** were isolated manually under an optical microscope upon washing of the residue containing single crystals with CH_2Cl_2, followed by CH_3CN wash (Supporting Information, Figure S11). Yield: 10% in the case of $\mathbf{L^1}$and 7% in the case of $\mathbf{L^2}$. Anal. Calcd for $C_{12}H_{37}Cl_3Hg_8O_{12}S_{13}$: C, 5.76; H, 1.49; S, 16.66. Found: C, 5.82; H, 1.36; S, 16.46. IR data (KBr pellet, cm^{-1}): 3456.2(w), 3012.6(w), 2933.5(s), 1635.52(w), 1423.37(s), 1307.65(s), 1099.35(s), 1081.99(s), 960.48(s), 682.75(w), 621.04(s). ESI-MS [positive ion mode in dimethyl sulfoxide (DMSO)/CH_3CN] data. Calcd for $[Hg_8S(SCH_3)_{12}][ClO_4]_2[HClO_4]$: *m*/*z* 2501.35. Found: *m*/*z*542.07 with expected isotope distribution patterns calculated for $[Hg_2(SCH_3)_3]^+$ (calcd *m*/*z* 542.16; Supporting Information, Figure S12).

X-ray Measurement and Structure Determination. The crystallographic data and details of data collection for *syn*-$\mathbf{L^1}$, *anti*-$\mathbf{L^1}$, $\mathbf{L^2}$, $\mathbf{L^3}$, and **1** are given in Table 1. In each case, a crystal of suitable size was selected from the mother liquor, immersed in paratone oil, then mounted on the tip of a glass fiber, and cemented using epoxy resin. Intensity data for all five crystals were collected using Mo Kα (λ = 0.7107 Å) radiation on a Bruker SMART APEX diffractometer equipped with a CCD area detector at 100 K. The data integration and reduction were processed with *SAINT*[13a] software. An empirical absorption correction was applied to the collected reflections with *SADABS*.[13b] Structures were solved by direct methods using *SHELXTL*[14] and were refined on F^2 by a full-matrix least-squares technique using the *SHELXL-97*[15] program package. Graphics were generated using *PLATON*[16] and *MERCURY 1.3*.[17] In all cases, non-hydrogen atoms were treated anisotropically, and all of the hydrogen atoms attached with carbon atoms were geometrically fixed. In $\mathbf{L^3}$, the hydrogen atom attached to the oxygen atom was located from the Fourier map and the other hydrogen atoms were geometrically fixed.

Optical Studies. Experiments on colorimetric sensing (visual detection) were carried out using $\mathbf{L^1}$−$\mathbf{L^3}$ (1×10^{-3} M) in

(11) (a) Matinez-Máñez, R.; Espinosa, A.; Tárraga, A.; Molina, P. *Org. Lett*. **2005**, *7*, 5869–5872. (b) Delavaux-Nicot, B.; Maynadié, J.; Lavabre, D.; Fery-Forgues, S. *Inorg. Chem*. **2006**, *45*, 5691–5702. (c) Basurto, S.; Riant, O.; Moreno, D.; Rojo, J.; Torroba, T. *J. Org. Chem*. **2007**, *72*, 4673–4688. (d) Willener, Y.; Joly, K. M.; Moody, C. J.; Tucker, J. H. R. *J. Org. Chem*. **2008**, *73*, 1225–1233. (e) Molina, P.; Tárraga, A.; Caballero, A. *Eur. J. Inorg. Chem*. **2008**, 3401–3417. (f) Zapata, F.; Caballero, A.; Espinosa, A.; Tárraga, A.; Molina, P. *J. Org. Chem*. **2009**, *74*, 4787–4796. (g) Romero, T.; Caballero, A.; Espinosa, A.; Tárraga, A.; Molina, P. *Dalton Trans*. **2009**, 2121–2129. (h) Barlow, S.; Bunting, H. E.; Ringham, C.; Green, J. C.; Bublitz, G. U.; Boxer, S. G.; Perry, J. W.; Marder, S. R. *J. Am. Chem. Soc*. **1999**, *121*, 3715–3723. (i) Yamaguchi, Y.; Ding, W.; Sanderson, C. T.; Borden, M. L.; Morgan, M. J.; Kutal, C. *Coord. Chem. Rev*. **2007**, *251*, 515–524.

(12) (a) Dieter, R. K. *Tetrahedron* **1986**, *42*, 3029–3096. (b) Junjappa, H.; Ila, H.; Asokan, C. V. *Tetrahedron* **1990**, *46*, 5423–5506. (c) Elgemeie, G. H.; Sayed, S. H. *Synthesis* **2001**, 1747–1771. (d) Bi, X.; Dong, D.; Liu, Q.; Pan, W.; Zhao, L.; Li, B. *J. Am. Chem. Soc*. **2005**, *127*, 4578–4579. (e) Zhang, Q.; Sun, S.; Hu, J.; Liu, Q.; Tan, J. *J. Org. Chem*. **2007**, *72*, 139–143. (f) Gill, S.; Kocienski, P.; Kohler, A.; Pontiroli, A.; Liu, Q. *Chem. Commun*. **1996**, 1743–1744. (g) Anabha, E. R.; Asokan, C. V. A. *Synthesis* **2006**, 151–155. (h) Rao, H. S. P.; Vasantham, K. *J. Org. Chem*. **2009**, *74*, 6847–6850. (i) Rao, H. S. P.; Sivakumar, S. *J. Org. Chem*. **2005**, *70*, 4524–4527. (j) Rao, H. S. P.; Sakthikumar, L.; Vanitha, S.; Siva Kumar, S. *Tetrahedron Lett*. **2003**, *44*, 4701–4704.

(13) (a) *SAINT and XPREP*, 5.1 ed.; Siemens Industrial Automation Inc.: Madison, WI, **1995**. Sheldrick, G. M. (b) *SADABS, Empirical Absorption Correction Program*; University of Göttingen: Göttingen, Germany, **1997**.

(14) Sheldrick, G. M. *SHELXTL Reference Manual: Version 5.1*; Bruker AXS: Madison, WI, **1997**.

(15) Sheldrick, G. M. *SHELXL-97: Program for Crystal Structure Refinement*; University of Göttingen: Göttingen, Germany, **1997**.

(16) Spek, A. L. *PLATON-97*; University of Utrecht: Utrecht, The Netherlands, **1997**.

(17) *Mercury 1.3 Supplied with Cambridge Structural Database*; CCDC: Cambridge, U.K., 2003−2004.

Table 1. Crystallographic Parameters of *syn*-$\mathbf{L^1}$, *anti*-$\mathbf{L^1}$, $\mathbf{L^2}$, $\mathbf{L^3}$, and **1**

param	syn polymorph $\mathbf{L^1}$	anti polymorph $\mathbf{L^1}$	$\mathbf{L^2}$	$\mathbf{L^3}$	**1**
empirical formula	$C_{20}H_{22}FeO_2S_4$	$C_{20}H_{22}FeO_2S_4$	$C_{15}H_{16}FeOS_2$	$C_{14}H_{14}FeOS_2$	$C_{12}H_{36}Cl_3Hg_8O_{12}S_{13}$
fw	478.47	478.47	332.25	318.24	2500.26
cryst syst	monoclinic	monoclinic	monoclinic	orthorhombic	trigonal
space group	$P2(1)/c$	$P2(1)/c$	$P2(1)/c$	$Pbca$	$R\bar{3}$
a (Å)	13.5321(10)	12.0897(11)	10.8726(17)	9.9223(4)	11.1963(12)
b (Å)	10.9902(8)	7.5984(7)	12.3291(19)	9.7972(4)	11.1963(12)
c (Å)	14.7987(11)	11.7415(11)	11.8362(19)	27.6193(11)	30.160(6)
α (deg)	90.00	90.00	90.00	90.00	90.00
β (deg)	107.4280(10)	109.437(2)	115.368(3)	90.00	90.00
γ (deg)	90.00	90.00	90.00	90.00	120.00
V (Å^3)	2099.8(3)	1017.13(16)	1433.6(4)	2684.89(19)	3274.2(8)
Z	4	2	4	8	3
d_{calcd} (g cm^{-3})	1.513	1.562	1.539	1.575	3.804
cryst size (mm^3)	0.22 × 0.20 × 0.16	0.20 × 0.15 × 0.12	0.22 × 0.19 × 0.14	0.14 × 0.12 × 0.10	0.18 × 0.18 × 0.18
diffractometer	Smart CCD	Smart CCD	Smart CCD	Smart CCD	Smart CCD
F(000)	992	496.0	688.0	1312	3309
μ(Mo Kα) (mm^{-1})	1.129	1.165	1.331	1.417	28.871
T (K)	100(2)	100(2)	100(2)	100(2)	100(2)
θ_{max} (deg)	25	24.990	25.0	22.2	24.990
reflcns collected	19 533	9345	16 304	18 272	10 216
indep reflcns	3686	1786	2526	1686	1291
param refined	332	168	236	165	79
R1, wR2	0.0251, 0.0692	0.0345, 0.0707	0.0233, 0.0631	0.0302, 0.0763	0.0335, 0.0770
GOF (F^2)	1.031	0.980	1.09	1.01	1.072

CH_3CN in the presence of 10 equiv of metal ions at room temperature. In a typical experiment, 3 mL of (1×10^{-3} M) ferrocenylchalcone was taken in a vial and 10 equiv of a metal ion (1×10^{-2} M) solution was added in one shot to detect the color change. The effects of different metal ions on the color changes were captured using a digital camera where optical photographs were taken 10 min after the addition of metal ions. Spectroscopic changes upon the addition of metal salts to the ligands were recorded using a UV/vis/NIR scanning spectrophotometer. In these experiments, 5×10^{-5} M ($\mathbf{L^1}$) and 1×10^{-4} M ($\mathbf{L^2}$ and $\mathbf{L^3}$) ligand and 1×10^{-2} M metal ion stock solutions were prepared in dry CH_3CN. Spectra were routinely acquired at 25 °C in a 1-cm-path-length quartz cuvette with a volume of 3.5 mL. To calculate molar extinction coefficients (ε) in the cases of $\mathbf{L^1}$ and $\mathbf{L^2}$ in the presence of Hg^{2+}, 2.5 mL of ferrocenylchalcone was taken in the cuvette and 10 equiv of Hg^{2+} (1×10^{-2} M) was added. The optical density was measured at a particular wavelength. UV/vis titration experiments of $\mathbf{L^1}$ and $\mathbf{L^2}$ in the presence of Hg^{2+} were carried out with freshly prepared stock solutions of ligands and metal salts in dry CH_3CN.

Electrochemical Studies. The CV measurements were performed on a potentiostat with a conventional three-electrode configuration consisting of platinum working and auxiliary electrodes and an Ag/Ag^+, NaCl (satd), reference electrode. The experiments were carried out with a 1×10^{-3} M solution of $\mathbf{L^1}$ and $\mathbf{L^2}$ in dry CH_3CN containing 0.1 M [(n-Bu)$_4$N]ClO_4 as the supporting electrolyte. Deoxygenation of the solutions was achieved by bubbling nitrogen for at least 10 min, and the working electrode was cleaned after each run. The CVs were recorded with a scan rate of 100 mV s^{-1}.

Results and Discussion

Syntheses. The general synthetic route for thiomethoxyferrocenylchalcone derivatives is based on a two-step sequence: a nucleophilic attack of the enolate anion with CS_2, followed by methylation of the potassium salt of ferrocenylsulfanyl-2-propen-1-one.[10c] On the basis of this approach, $\mathbf{L^1}$ having bis(ketene) dithiomethyl acetal is designed and synthesized from 1,1′-diacetylferrocene as a backbone in good yield (Scheme 1). Depending upon the choice of solvent systems, $\mathbf{L^1}$ is crystallized as a syn polymorph (Table 1 and Figure 1a) in a CH_2Cl_2/diethyl ether binary mixture and as an anti polymorph (Table 1 and Figure 1b) in a CH_2Cl_2/petroleum ether binary mixture. Ferrocene and ferrocene derivatives are well-known compounds for not only their high redox activity but also their unique rotational motion. The two cyclopentadienyl rings of ferrocene have a low rotational energy barrier, which allows almost free rotation of the rings. In the case of $\mathbf{L^1}$, upon judicious choice of different binary solvent systems, we could capture both syn and anti polymorphs of $\mathbf{L^1}$, where both crystallized in the $P2_1/c$ space group. Isolation of syn and anti polymorphs clearly demonstrates the conformational flexibility of $\mathbf{L^1}$. In both cases, two cyclopentadienyl rings adopted a staggered conformation where *anti*-$\mathbf{L^1}$ consisted of a crystallographically imposed inversion center at the iron atom. $\mathbf{L^2}$ and $\mathbf{L^3}$ were synthesized from monoacetylferrocene in good yields for comparative colorimetric sensing of Hg^{2+} with $\mathbf{L^1}$. Monoketene dithiomethyl acetal, $\mathbf{L^2}$, is designed to study the effect of bis- versus monofunctionality and/or any role of conformational freedom toward Hg^{2+} sensing. $\mathbf{L^2}$ is also characterized by a single-crystal X-ray diffraction study (Table 1 and Figure 1c). Further, to understand the role of the dithiomethyl acetal group in the sensing of metal ions, we have synthesized thiomethyl hemiacetal, $\mathbf{L^3}$, having one thiol and one thiomethoxy group as substituents in moderate yield and also characterized by a single-crystal X-ray diffraction study (Table 1 and Figure 1d). The single-crystal X-ray structure of $\mathbf{L^3}$ shows the location of the hydrogen atom on the oxygen atom of the chalcone moiety, and it is due to the presence of keto−enol tautomerism in this system. The solvent diffusion method allowed us to isolate **1** in very low yield, which could be regarded as one of the products upon reaction between $\mathbf{L^1}$/$\mathbf{L^2}$ and Hg^{2+}. The major fraction of the final blackish residue obtained during crystallization could be mixtures of unidentified decomposed products.

Visual Detection of Hg^{2+}. When 10 equiv of different metal ions (Li^+, Na^+, Ca^{2+}, Mg^{2+}, Cr^{2+}, Mn^{2+}, Fe^{2+}, Co^{2+}, Ni^{2+}, Cu^{2+}, Zn^{2+}, Cd^{2+}, Hg^{2+}, and Au^{3+}) are separately added to the CH_3CN solution of bis(ketene)

dithiomethyl acetal, $\mathbf{L^1}$ (1×10^{-3} M), having four thiomethoxy substitutents on two chalcone-functionalized arms on ferrocene, shows a color change from orange to purple only in the case of Hg^{2+}, whereas other ions do not show any appreciable change in color under similar experimental conditions (Figure 2a). The selective color change in the case of Hg^{2+} with $\mathbf{L^1}$ can be used for the "naked-eye" detection of this particular metal ion in solution. The sensing ability of $\mathbf{L^1}$ toward Hg^{2+} in solution is independent of the syn or anti conformation of the

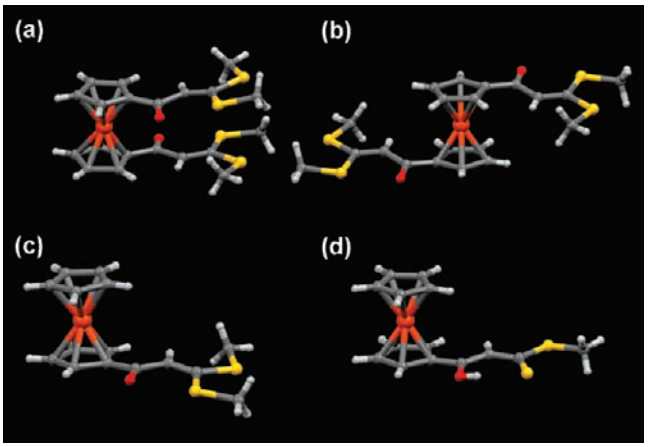

Figure 1. Perspective views of (a) *syn*-$\mathbf{L^1}$, (b) *anti*-$\mathbf{L^1}$, (c) $\mathbf{L^2}$, and (d) $\mathbf{L^3}$.

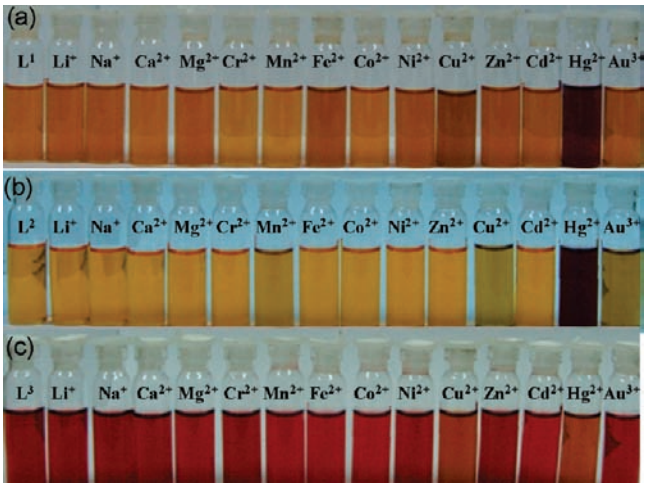

Figure 2. Changes in the color of 1×10^{-3} M solutions of (a) $\mathbf{L^1}$, (b) $\mathbf{L^2}$, and (c) $\mathbf{L^3}$ with 10 equiv of various metal ions in CH_3CN.

Scheme 1. Syntheses of Ferrocenylchalcones $\mathbf{L^1}$–$\mathbf{L^3}$

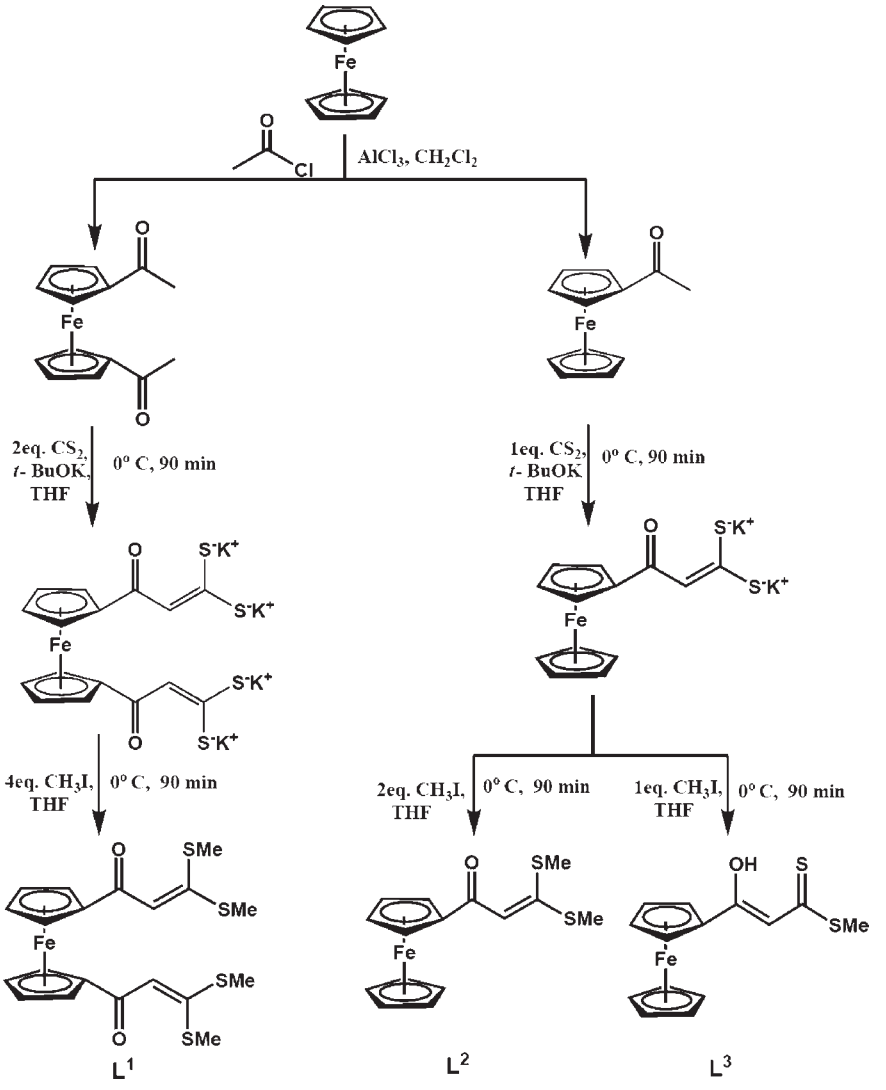

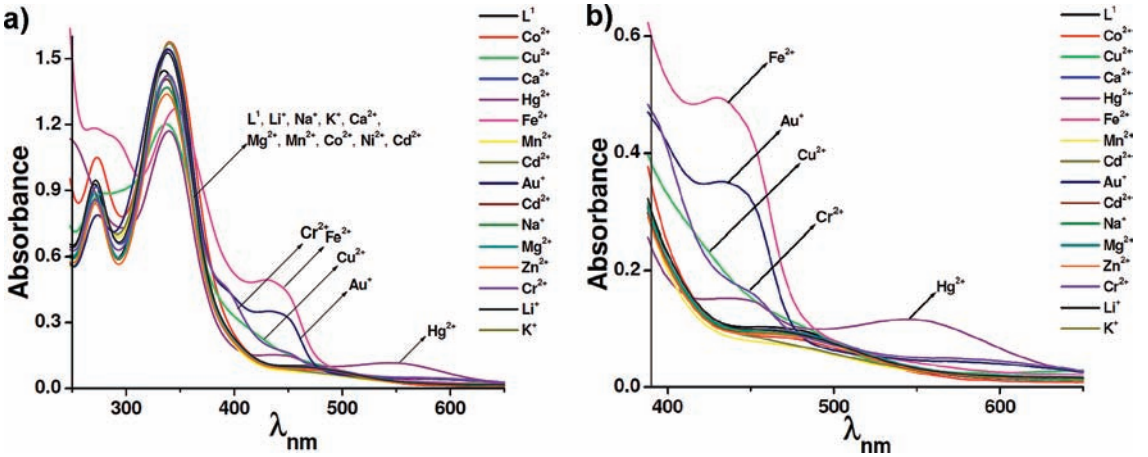

Figure 3. (a) UV/vis spectra of 5×10^{-5} M solutions of $\mathbf{L^1}$ and $\mathbf{L^1}$ with 10 equiv of various metal ions in CH_3CN. (b) Expanded form of part a.

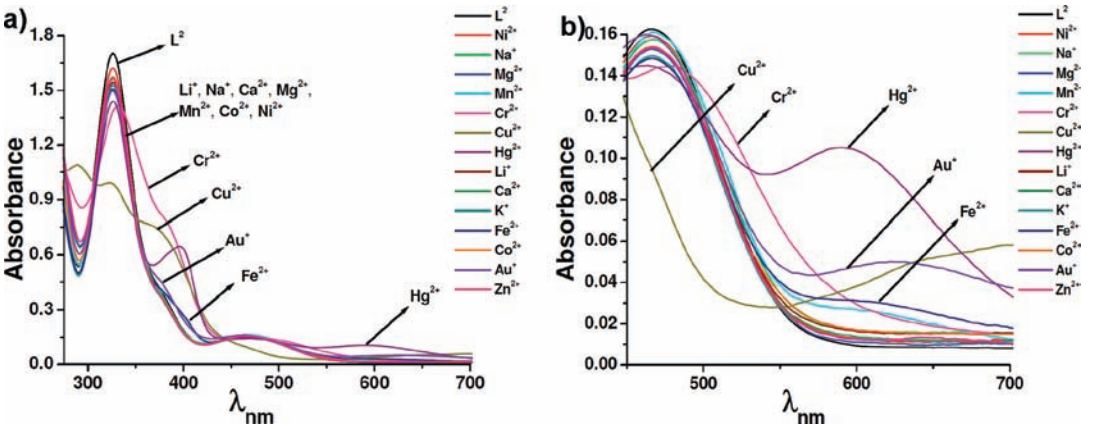

Figure 4. (a) UV/vis spectra of 1×10^{-4} M solutions of $\mathbf{L^2}$ and $\mathbf{L^2}$ with 10 equiv of various metal ions in CH_3CN. (b) Expanded form of part a.

ligand, suggesting that conformational equilibrium exists in the solution state. A similar selective color change is also observed in the case of Hg^{2+} with the monoketene dithiomethyl acetal, $\mathbf{L^2}$, having two thiomethoxy substitutents on one chalcone-functionalized arm (Figure 2b). Thus, ferrocenylchalcones $\mathbf{L^1}$ and $\mathbf{L^2}$ represent a new family of Hg^{2+} sensors in CH_3CN. In the case of monoketene dithiomethyl hemiacetal, $\mathbf{L^3}$, where one of the thiomethoxy groups of $\mathbf{L^2}$ is replaced by a thiol functionality, fails to show any detectable color change with Hg^{2+} (Figure 2c). This suggests the necessity of the dithiomethylacetal functionality of the chalcone moiety on the ferrocene backbone for selective sensing toward Hg^{2+}.

UV/Vis Absorption Spectroscopy Studies. Figure 3 shows the UV/vis spectra of $\mathbf{L^1}$ (5×10^{-5} M in CH_3CN) and $\mathbf{L^1}$ in the presence of 10 equiv of various metal ions (Li^+, Na^+, Ca^{2+}, Mg^{2+}, Cr^{2+}, Mn^{2+}, Fe^{2+}, Co^{2+}, Ni^{2+}, Cu^{2+}, Zn^{2+}, Cd^{2+}, Hg^{2+}, and Au^{3+}). The UV/vis spectrum of $\mathbf{L^1}$ shows an absorption band at 344 nm, which can be attributed to a high-energy ligand-centered $\pi-\pi^*$ electronic transition ($\mathbf{L}-\pi^*$) (HE band), and a relatively weak low-energy absorption band at 480 nm ($\varepsilon = 1220$ M^{-1} cm^{-1}), which may be attributed to a metal−ligand charge transfer (MLCT; Figure S13 of the Supporting Information). There is the possibility of Fe^{II} d−d degenerate transitions buried under the MLCT band. This is in accordance with already reported ferrocene-based ligands.[11] During the addition of 10 equiv of various metal ions, only Hg^{2+} shows the appearance of a new peak (Figure 3b) at 565 nm ($\varepsilon = 3920$ M^{-1} cm^{-1}).

In the case of $\mathbf{L^2}$ (1×10^{-4} M in CH_3CN), a high-energy absorption band is observed at 326 nm along with a weaker low-energy absorption band at 466 nm (Figure 4). Relatively lower wavelength absorption bands in this case, compared to $\mathbf{L^1}$, are due to less conjugation around the chalconyl functionality in $\mathbf{L^2}$. In the presence of 10 equiv of various metal ions, the appearance of a new peak at 600 nm ($\varepsilon = 1140$ M^{-1} cm^{-1}) is observed, with Hg^{2+} similar to $\mathbf{L^1}$ but at a higher wavelength (~35 nm higher; Figure 4). Upon a closer look at the UV/vis spectra of $\mathbf{L^2}$ with all other ions (Figure 4b), only Au^{3+} shows a new peak at 620 nm with a lower molar extinction coefficient ($\varepsilon = 550$ M^{-1} cm^{-1}), but in the case of $\mathbf{L^1}$, no such peak is observed with Au^{3+}. A slight change in color is evident in the presence of Au^{3+} with $\mathbf{L^2}$ (Figure 2), and that could be due to the absorbance band at 620 nm with a lower molar extinction coefficient value. Although both $\mathbf{L^1}$ and $\mathbf{L^2}$ show colorimetric sensing of Hg^{2+} in CH_3CN, $\mathbf{L^1}$ shows a higher molar extinction coefficient as well as noninterference of Au^{3+} than that of $\mathbf{L^2}$.

$\mathbf{L^3}$ (1×10^{-4} M in CH_3CN) shows a high-energy absorption band at 388 nm and a weaker low-energy absorption band at 512 nm (Figure 5) and relatively longer wavelength than $\mathbf{L^1}$ and $\mathbf{L^2}$ because of the existence of keto−enol tautomerism on the chalconyl functionality.

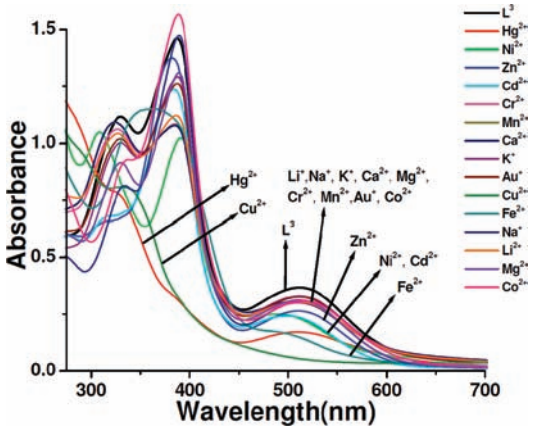

Figure 5. UV/vis spectra of 1×10^{-4} M solutions of $\mathbf{L^3}$ and $\mathbf{L^3}$ with 10 equiv of various metal ions in CH_3CN.

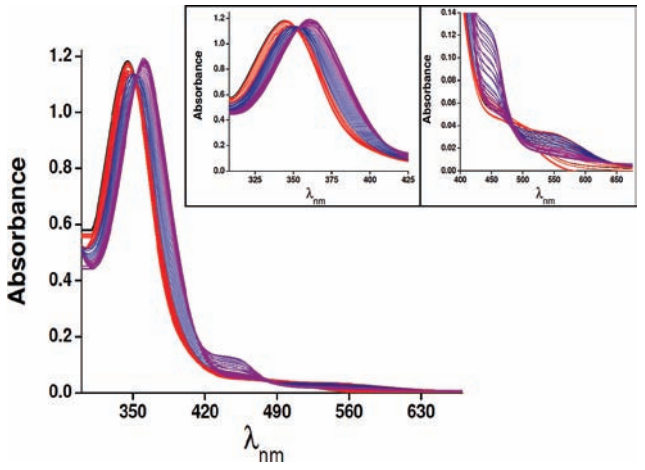

Figure 6. UV/vis titration profile of $\mathbf{L^1}$ (5×10^{-5} M) with Hg^{2+} of up to 2 equiv in CH_3CN. The color code represents the addition of Hg^{2+}: red, 0−0.5 equiv; blue, 0.5−1 equiv; purple, 1−2 equiv.

In the presence of 10 equiv of various metal ions in an acetonitrile solution, no appreciable change in the absorbance spectra is observed (Figure 5) even with Hg^{2+}.

In the UV/vis titration study of $\mathbf{L^1}$, the gradual addition of Hg^{2+} up to 0.5 equiv causes the appearance of a new peak at 565 nm with a concomitant decrease in the HE band at 344 nm and the LE band at 480 nm (Figures 6 and 7, red spectra). These spectral changes could be due to the binding of Hg^{2+} with the sulfur atoms of $\mathbf{L^1}$. The increase in the absorption band at 565 nm upon the gradual addition of 0.5 equiv of Hg^{2+} is indicative of the formation of a 1:2 complex ($Hg^{2+}/\mathbf{L^1}$; Figure 8a). A further addition (above 0.5 equiv) causes a decrease in the intensity at 565 nm and a gradual red shift of the 344 nm HE band to 356 nm, with up to 1 equiv of Hg^{2+} to generate a new absorption band at 444 nm (Figures 6 and 7, blue spectra). This indicates the formation of a new complex in the reaction mixtures. During titration with 0.5−1.0 equiv of Hg^{2+}, the inflection point in Job's plot shows at 0.5 with respect to 444 nm, indicating the existence of a 1:1 ($\mathbf{L^1}/Hg^{2+}$) complex in solution (Figure 8b). A further addition of Hg^{2+} above 1 equiv leads to a gradual red shift of the 356 nm band to 362 nm upon the addition of 2 equiv of Hg^{2+} (Figures 6 and 7). It is clear from Figures 6 and 7 that, with saturation of the peak at 362 nm, the peak at 444 nm disappeared. This might be attributed to the mercury thiol charge-transfer band that is formed by decomposition of the thiomethoxy groups of $\mathbf{L^1}$ assisted by Hg^{2+}.

Further well-defined isosbestic points at 352, 471, and 486 nm during UV/vis titration studies clearly indicate the presence of a unique complex in equilibrium with the free receptor, whereas titration of $\mathbf{L^2}$ with increasing concentration of Hg^{2+} leads to the appearance of a new peak at 600 nm with up to 1 equiv of Hg^{2+} with a concomitant decrease at 326 and 466 nm (Figure 9a) and well-defined isosbestic points at 307, 343, 446, and 532 nm. Job's plot shows the existence of a 1:1 ($\mathbf{L^2}/Hg^{2+}$) complex in solution (Figure 9b). Although $\mathbf{L^2}$ shows that the color changes from orange to purple similar to $\mathbf{L^1}$, the appearance of a new peak at a different wavelength without any spectral shift is unlike the situation in $\mathbf{L^1}$ (where spectral shifts are observed along with a new peak at 565 nm).

Electrochemical Studies. We have performed CV experiments of $\mathbf{L^1}$ in the presence of Hg^{2+} to study the reversibility and the change in the oxidation potential of $\mathbf{L^1}$ (Figure 10). The CV of the receptor $\mathbf{L^1}$ showed a reversible oxidation potential at ca. +0.845 V, which is higher than the oxidation potential of ferrocene (+0.49 V vs NHE). Upon the addition of Hg^{2+} of up to 0.5 equiv, there is no appreciable change in the reversibility and/or shift of the oxidation potential (Figure 10). A further addition of Hg^{2+} of up to 1 equiv causes a decrease in the current intensity with a reversible oxidation wave and of more than 1 equiv of Hg^{2+} causes an irreversible wave. The change in the CV spectra upon the gradual addition of Hg^{2+} also supports the UV/vis titration data. The irreversible nature beyond 1 equiv suggests the disappearance of $\mathbf{L^1}$ by selective Hg^{2+}-prompted chemodosimetric desulfurization. The intensity of the current peak slowly decreases with an increase in the concentration of Hg^{2+}, which could be due to the cleavage of the C−S bond and consequent deposition of sulfur or thiolate on the electrode. On the other hand, time-dependent ^1H NMR spectral changes of $\mathbf{L^1}$ in the presence of Hg^{2+} indicate the existence of a ferrocene unit in solution (Supporting Information, Figure S14).

The CV of the receptor $\mathbf{L^2}$ showed a reversible oxidation potential at ca. +0.680 V (Figure 11), which is lower than that of $\mathbf{L^1}$. This is due to the presence of a mono versus bis electron-withdrawing ketene *S*,*S*-acetal(s) functionality in the cases of $\mathbf{L^2}$ and $\mathbf{L^1}$, respectively. Upon the gradual addition of Hg^{2+} to the solution of $\mathbf{L^2}$, the disappearance of the reversible voltammogram is observed with an increase in the current intensity (Figure 11). This also supports selective Hg^{2+}-prompted chemodosimetric desulfurization in this case too.

Crystal Structure. In order to characterize the product formed during chemodosimetric sensing of Hg^{2+} by $\mathbf{L^1}$ and $\mathbf{L^2}$, we tried crystallization of the reaction products of $\mathbf{L^1}$ or $\mathbf{L^2}$ and Hg^{2+} in various ways. We could isolate purple crystals of **1** as one of the products suitable for a single-crystal X-ray study by slow diffusion of $Hg(ClO_4)_2$ in CH_3CN with $\mathbf{L^1}$ or $\mathbf{L^2}$ in CH_2Cl_2 after 1 week. The solid-state structural analysis of **1** showed the formation of a distorted cuboctahedron sulfide-encapsulated (μ_8-S) mercury thiolate cluster (Figure 12). It indeed proves that the cluster formation is independent of the number of

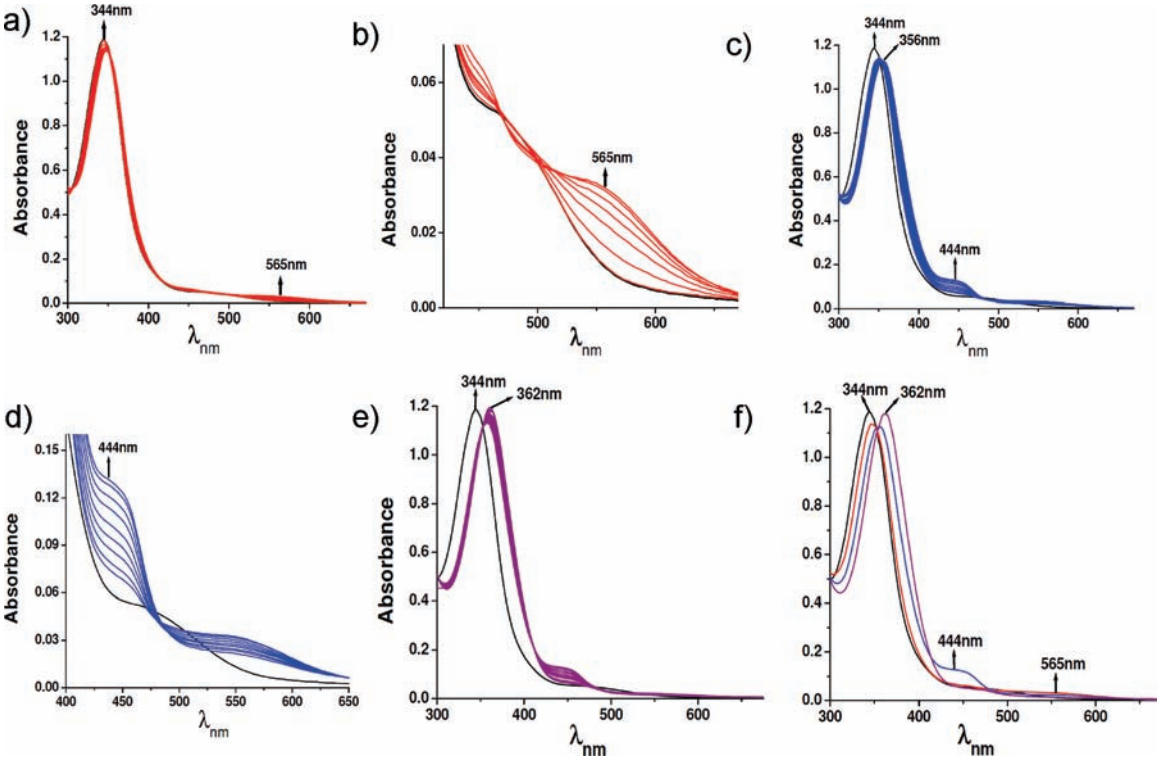

Figure 7. UV/vis titration profile of $\mathbf{L^1}$ (5×10^{-5} M) with the range of Hg^{2+} in CH_3CN: (a) 0−0.5 equiv; (b) expanded spectrum of part a; (c) 0.5−1 equiv; (d) expanded spectrum of part c; (e) 1−2 equiv; (f) 0, 0.5, 1, and 2 equiv of Hg^{2+}. The color code represents the addition of Hg^{2+}: red, 0−0.5 equiv; blue, 0.5−1 equiv; purple, 1−2 equiv.

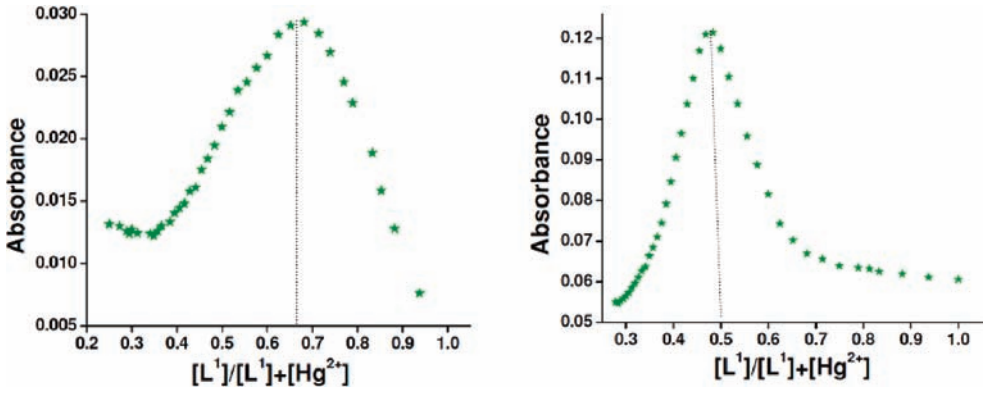

Figure 8. Job's plot of the titration profile of $\mathbf{L^1}$ (5×10^{-5} M) with Hg^{2+} in CH_3CN and showing (a) a $\mathbf{L^1}/Hg^{2+}$ (2:1) complex with respect to 565 nm and (b) $\mathbf{L^1}/Hg^{2+}$ (1:1) with respect to 462 nm.

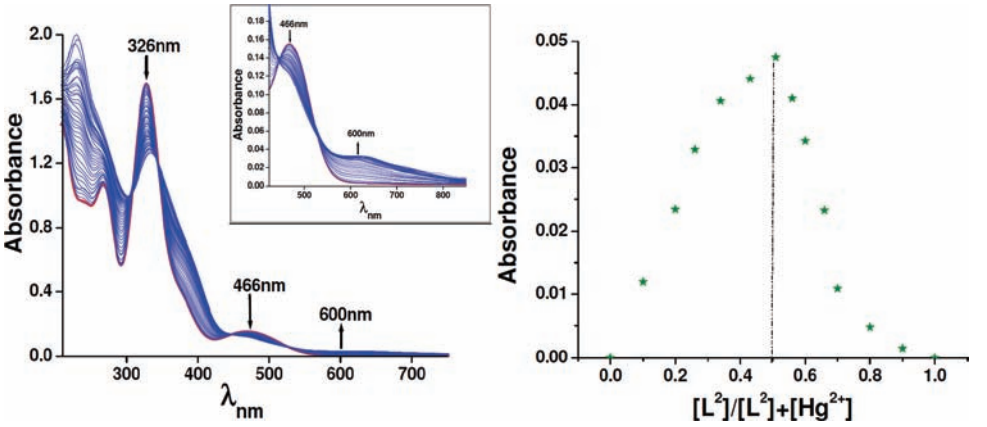

Figure 9. (a) UV/vis titration profile of $\mathbf{L^2}$ (5×10^{-5} M) with Hg^{2+} in CH_3CN. Inset: expanded spectrum from 400 to 800 nm. (b) Job's plot of the titration profile of $\mathbf{L^2}$ (5×10^{-5} M) with Hg^{2+} in CH_3CN showing $\mathbf{L^2}/Hg^{2+}$ (1:1) with respect to 600 nm.

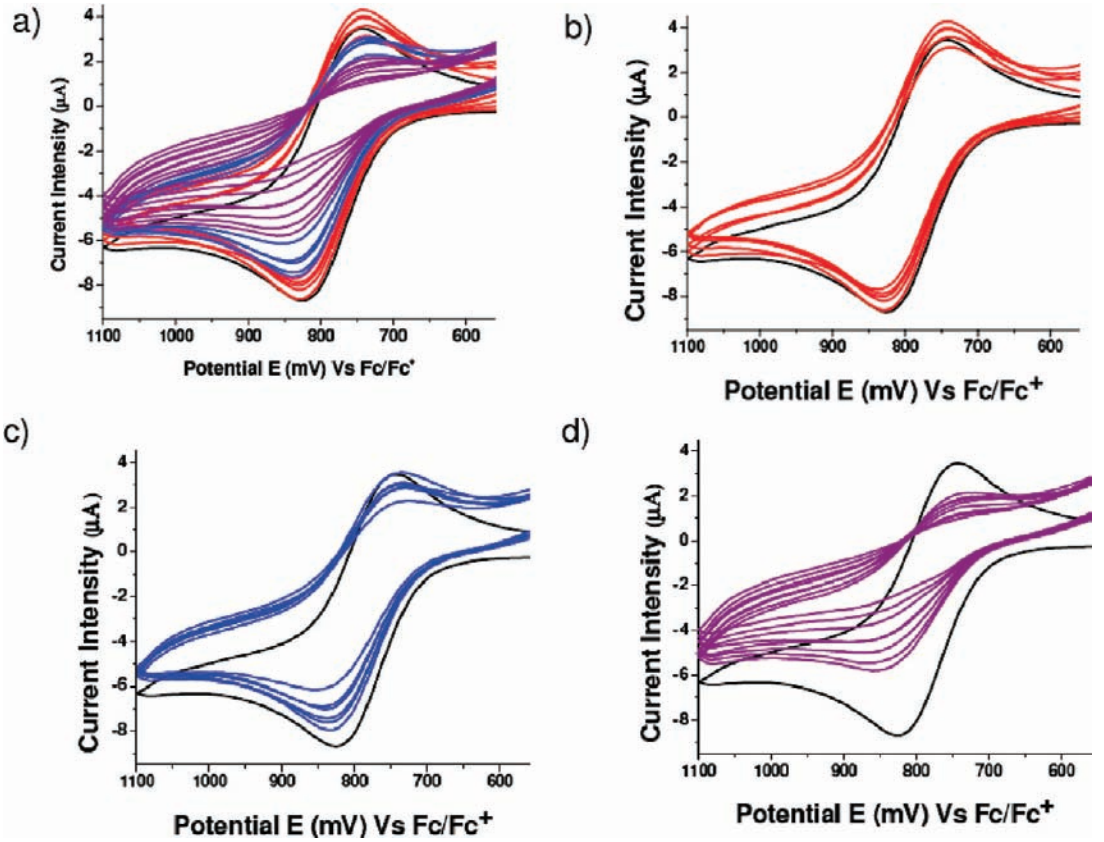

Figure 10. CV diagram of $\mathbf{L^1}$ (1×10^{-3} M) in CH_3CN using 0.1 M $[(n\text{-}Bu)_4N]ClO_4$ as the supporting electrolyte with the gradual addition of Hg^{2+}: (a) up to 0−2 equiv of Hg^{2+}; (b) 0−0.5 equiv of Hg^{2+}; (c) 0.5−1 equiv of Hg^{2+}; (d) 1−2 equiv of Hg^{2+}. The color code represents the addition of Hg^{2+}: red, 0−0.5 equiv; blue, 0.5−1 equiv; purple, 1−2 equiv.

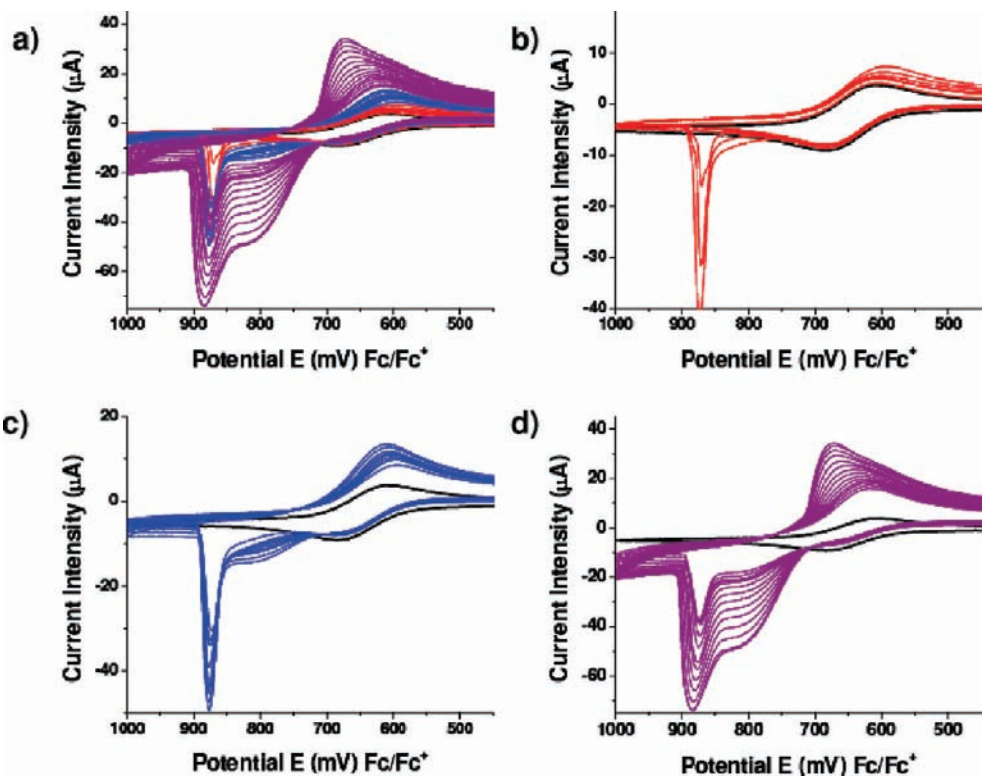

Figure 11. CV diagram of $\mathbf{L^2}$ (1×10^{-3} M) in CH_3CN using 0.1 M $[(n\text{-}Bu)_4N]ClO_4$ as the supporting electrolyte with the gradual addition of Hg^{2+}: (a) combined voltammogram upon the addition of 0−2 equiv of Hg^{2+}, (b) 0−0.5 equiv of Hg^{2+}, (c) 0.5−1 equiv of Hg^{2+}, and (d) 1−2 equiv of Hg^{2+}. The color code represents the addition of Hg^{2+}: red, 0−0.5 equiv; blue, 0.5−1 equiv; purple, 1−2 equiv.

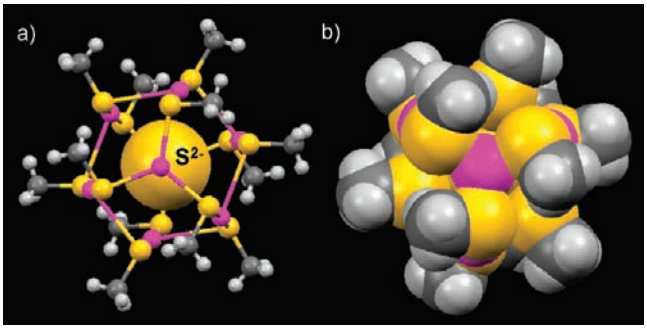

Figure 12. Perspective view of $[Hg_8S(SCH_3)_{12}]^{2+}$cluster **1**: (a) ball-and-stick model (encapsulated sulfide is in the spacefill model); (b) spacefill model. Color code: pink, mercury; yellow, sulfur. Perchlorates were omitted for clarity.

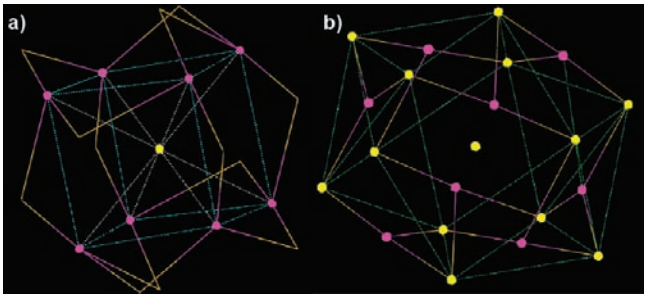

Figure 13. Perspective view of $[Hg_8S(SCH_3)_{12}]^{2+}$ cluster **1**: (a) Hg_8 cube; (b) cuboctahedran cage. Hydrogen and carbon atoms and ClO_4^- were omitted for clarity. Color code: pink, mercury; yellow, sulfur. Perchlorates were omitted for clarity.

arms as well as the conformations. One of the perchlorates was assigned as perchloric acid based on TGA data (Supporting Information, Figure S15). The cluster consists of eight Hg^{2+} ions that form a cubelike array (Hg_8 cube; Figure 13a) with a set of Hg···Hg distances of 3.661, 3.662, and 3.817 Å. These mercury atoms of the cube are connected by 12 thiomethoxy bridges (Figure 13). A total of 12 sulfur atoms of thiomethoxy units represents 12 vertices of an cuboctahedron cage where a S^{2-}-encapsulated Hg_8 cube occupies its inner volume (Figure 13b).

The S^{2-} ion, i.e., S7 located at the center of the cage, is weakly coordinated with eight Hg^{2+} in a μ_8-S fashion as a cuboctahedron, where S7···Hg distances range from 3.236 to 3.240 Å (Figure 14).[18] The two bridge-head mercury atoms Hg1′ and Hg8′ are in an exo,exo conformation, where Hg^{2+} ions lie at 0.224 Å "in" from the planes consisting of S1′S2′S3′ and S10′S11′S12′, respectively, and 2.847 Å from the plane of the distorted oxygen atom (O11BO11BO11B) of the perchlorate ions (Figure 14).

Here Hg1′ and Hg8′ share the trigonal plane with three thiomethoxy bridges; encapsulated sulfide above and one perchlorate below the plane are coordinated to form the trigonal-bipyramidal geometry with Hg···S bond distances ranging from 2.478 to 2.479 Å and ∠S−Hg−S ranges from 119.17 to 119.21°. The encapsulated sulfide S7 lies between the two mercury atoms Hg1′ and Hg8′ with a Hg···S7 distance of 3.2387(9) Å and ∠Hg−S7−Hg of 179.97(13)° (Figure 15). The other six Hg^{2+} of the cluster

(18) (a) Ghosh, D.; Lee, K. H.; Demeler, B.; Pecoraro, V. L. *Biochemistry* **2005**, *44*, 10732–10740. (b) Qin, J.; Song, L.; Brim, H.; Daly, M. J.; Summers, A. O. *Microbiology* **2006**, *152*, 709–719. (c) Manceau, A.; Nagy, K. L. *Dalton Trans*. **2008**, 1421–1425.

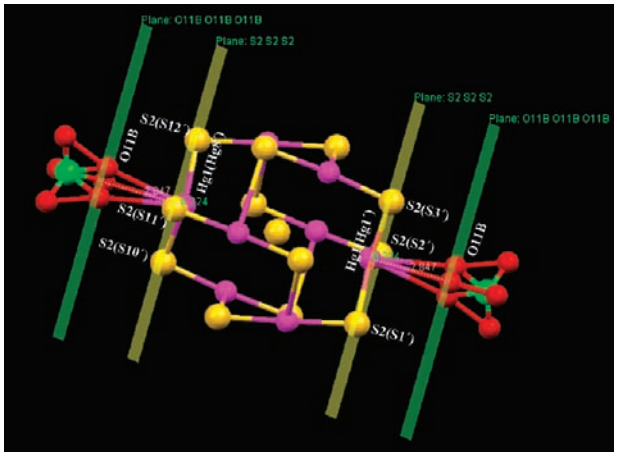

Figure 14. Crystallographic representation of cluster **1**.

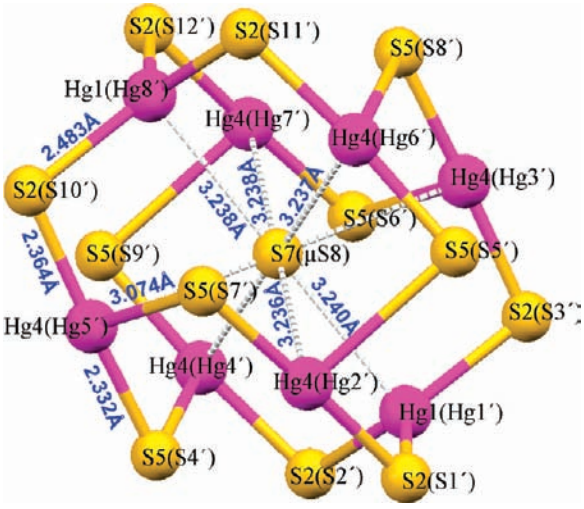

Figure 15. Perspective view of $[Hg_8S(SCH_3)_{12}]^{2+}$ cluster **1**. All hydrogen and carbon atoms and ClO_4^- were omitted for clarity. Color code: pink, mercury; yellow, sulfur. The labeling inside the parentheses is exclusively for the structural discussion, while the original atom numbering appears outside the parentheses.

are represented by Hg4 and are in tricoordination with a thiomethoxy sulfur in a distorted T-shaped trigonal-planar symmetry with one S2 and two S5 sulfur atoms. The detailed bond parameters for Hg2′ coordination are as follows: Hg2′···S1′ = 2.364(3) Å, Hg2′···S5′ = 3.074(4) Å, and Hg2′···S7′ = 2.332(3) Å with bond angles ∠S1′−Hg2′−S5′ = 83.64(9)°, ∠S1′−Hg2′−S7′ = 175.97(13)°, and ∠S5′−Hg2′−S7′ = 98.27(9)° (Figure 15). The T-shaped geometry is the extreme case of trigonal distortion, which has been observed in other coordination compounds.[18,19] Further, the distorted planar configuration is also believed to be responsible for detoxification of Hg^{2+} in living cells.[18a,b] The fourth weak coordination of Hg2′ is fulfilled by the encapsulated sulfide S7, with a bond distance ranging

(19) (a) Tiekink, E. R. T. *Acta Crystallogr., Sect. C* **1987**, *43*, 448–450. (b) Fong, S.-W. A.; Yap, W. T.; Vittal, J. J.; Hor, T. S. A.; Henderson, W.; Oliver, A. G.; Rickard, C. E. F. *J. Chem. Soc., Dalton Trans*. **2001**, 1986–2002. (c) Chen, J.-X.; Zhang, W.-H.; Tang, X.-Y.; Ren, Z.-G.; Zhang, Y.; Lang, J.-P. *Inorg. Chem*. **2006**, *45*, 2568–2580. (d) Tang, X.-Y.; Yuan, R.-X.; Ren, Z.-G.; Li, H.-X.; Zhang, Y.; Lang, J.-P. *Inorg. Chem*. **2009**, *48*, 2639–2651. (e) Tang, X.-Y.; Li, H.-X.; Chen, J.-X.; Ren, Z.-G.; Lang, J.-P. *Coord. Chem. Rev*. **2008**, *252*, 2026–2049. (f) Tang, X.-Y.; Chen, J.-X.; Liu, G.-F.; Ren, Z.-G.; Zhang, Y.; Lang, J.-P. *Eur. J. Inorg. Chem*. **2008**, 2593–2600.

from 3.2373(8) to 3.2387(9) Å. A $[Hg_8S(SR)_{12}]^{2+}$ molecular unit in **1** is a representation of a sulfide-centered antifluorite-type lattice of a sulfur cuboctahedron and can be described as an ensemble of eight metal-filled distorted tetrahedra. Though the geometry of the hypothetical formula $[M_8S(SR)_{12}]^{2+}$ is explained in the literature,[5a,9] no example of $[M_8S(SR)_{12}]^{2+}$ is known in coordination chemistry; presumably the positive charge of the complex results in considerable destabilization.[5a] In the case of divalent cage complex **1**, probably the highly distorted trigonal-planar symmetry keeping the metals at the corners of the cube with distortion in the MS4 tetrahedra and stabilization of the positive charge of $[Hg_8S(SCH_3)_{12}]^{2+}$ by the coordination of two perchlorate anions at the bridge-head mercury atoms Hg1′ and Hg8′ leads to the existence of a cuboctahedron sulfide-encapsulated $[Hg_8S(SCH_3)_{12}]^{2+}$ cluster (Figure 14).

The optical spectrum of **1** in DMSO shows an absorption band at 255 nm with a visible tail of weak intensity (Supporting Information, Figure S11a). The absence of any clear absorption peak in the visible region does not explain the pink color of the single crystal of **1** (Supporting Information, Figure S11b). This may be due to the fact that complex **1** dissociates in a DMSO solution, which also corroborates with the mass spectral data (Supporting Information, Figure S12). On the other hand, the solid-state reflectance spectrum of **1** shows an absorption band at 295 nm along with a distinct peak at ∼575 nm (Supporting Information, Figure S11c). This clearly explains the pink color of **1** in the solid state, which may originate from the solid-state packing. The formation of cluster **1** upon reaction between $\mathbf{L^1}/\mathbf{L^2}$ and Hg^{2+} might involve a number of complicated reaction steps. Interaction of Hg^{2+} with the −SMe group of the ligand is clearly evident from the UV/vis, CV titration, and ^1H NMR studies. This interaction could be responsible for breaking the C−S bonds of the ferrocenylchalcones and also the formation of sulfide in the system.[20] Finally, **1** is formed via a number of complicated intermediate steps as one of the thermodynamically stable products with a very low yield.

Conclusion

In summary, we have developed simple thiomethoxyferrocenylchalcones $\mathbf{L^1}$ and $\mathbf{L^2}$ as a new family of ligands for selective colorimetric detection of Hg^{2+} by a chemodosimetric approach. We have also isolated a divalent mercury thiolate cluster $[Hg_8S(SCH_3)_{12}]^{2+}$ as one of the products formed upon reaction between Hg^{2+} and the receptor. The octanuclear metal(II) sulfide thiolate complexes containing metal−sulfur frames with thiolate-bridged complexes normally exist as complex anions.[20,21] The existence of cationic metal thiolate clusters is very rare.[7c,9] To the best of our knowledge, it represents the first structural evidence of any $[M_8S(SR)_{12}]^{2+}$ type of sulfide-encapsulated divalent metal thiolate cluster. The interesting approach of combining metals and main-group elements toward the isolation of these types of clusters could be useful for the synthesis of new materials and could provide a search for new coordinations and geometries. Presently, we are actively working to synthesize a similar type of cluster with other chalcone-based systems.

Acknowledgment. P.G. gratefully acknowledges the Department of Science and Technology (DST), New Delhi, India, for financial support. M.A. acknowledges CSIR, India, for SRF. The X-ray crystallography study was performed at the DST-funded National Single Crystal X-ray Diffraction Facility at the Department of Inorganic Chemistry, IACS.

Supporting Information Available: Experimental procedures and spectroscopic data for all new compounds, ^1H and ^{13}C NMR, ESI-MS, TGA, and UV/vis spectra, CV, and X-ray crystallographic data in CIF format. This material is available free of charge via the Internet at http://pubs.acs.org.

(20) (a) Burth, R.; Gelinsky, M.; Vahrenkamp, H. *Inorg. Chem.* **1998**, *37*, 2833–2836. (b) Dance, I. G. *Aust. J. Chem.* **1985**, *38*, 1391–1411. (c) Achim Müller, A.; Diemann, E.; Jostes, R.; Bögge, H. *Angew. Chem., Int. Ed. Engl.* **1981**, *20*, 934–955.

(21) (a) Gelinsky, M.; Vahrenkamp, H. *Z. Anorg. Allg. Chem.* **2002**, *628*, 1017–1021. (b) Guo, S.; Ding, E.; Liu, S.; Yin, Y. *J. Inorg. Biochem.* **1998**, *70*, 7–10. (c) Guo, S.; Ding, E.; Chen, H.; Yin, Y.; Li, X. *Polyhedron* **1999**, *18*, 735–740. (d) Dance, I. G. *J. Chem. Soc., Chem. Commun.* **1980**, 818–820. (e) Eichhöfer, A.; Fenske, D.; Pfistner, H.; Wunder, M. *Z. Anorg. Allg. Chem.* **1998**, *624*, 1909–1914.